



The large proportion of black carbon (BC)-containing aerosols in the urban atmosphere[☆]

Lu Chen^a, Fang Zhang^{a,*}, Peng Yan^b, Xinming Wang^c, Lu Sun^d, Yanan Li^b, Xiaochun Zhang^b, Yele Sun^e, Zhanqing Li^f

^a College of Global Change and Earth System Science, Beijing Normal University, Beijing, 100875, China

^b Meteorological Observation Center of China Meteorological Administration, Beijing, 100081, China

^c State Key Laboratory of Organic Geochemistry, Guangzhou Institute of Geochemistry, Chinese Academy of Sciences, Guangzhou, 510640, China

^d Department of Atmospheric Sciences, Texas A&M University, College Station, TX, USA

^e State Key Laboratory of Atmospheric Boundary Layer Physics and Atmospheric Chemistry, Institute of Atmospheric Physics, Chinese Academy of Sciences, Beijing, 100080, China

^f Earth System Science Interdisciplinary Center and Department of Atmospheric and Oceanic Science, University of Maryland, College Park, MD, USA

ARTICLE INFO

Article history:

Received 13 December 2019

Received in revised form

28 March 2020

Accepted 30 March 2020

Available online 5 April 2020

Keywords:

Black carbon (BC)-Containing particles

Number and mass fraction

Mixing state

Coating thickness

ABSTRACT

The accurate derivation of the proportion and absorption enhancement of black carbon (BC)-containing aerosols in the atmosphere is critical to assess their effect on air quality and climate. Here, using the field measured size-resolved volatility shrink factor, BC bulk mass concentration and the BC mass fraction in BC-containing particles in winter Beijing, we retrieved and quantified both the number and mass concentration of (1) non-BC, (2) internally mixed BC and (3) externally mixed BC of ambient fine aerosol particles. The reliability of the retrieval method has been evaluated by comparing with the simultaneously measured data. The number fraction of BC-containing particles accounts for 60–78% of ambient fine particles, with internally (both BC core and coating materials) and externally mixed BC of 51–64% and 9–23%, respectively. Only for nucleated particles on clean days, when nucleation is a major source of aerosol particles, did the non-BC component dominate (54%). A large amount of aerosols are BC-containing particles, with mass fraction of 32–52%, suggesting the dominant role of BC in elevating mass concentration of particulate matter (PM) in a polluted urban area. We also show that the BC particles are thickly coated with coating thickness (characterized by D_p/D_c , ratio of the BC diameter before and after heating at 300 °C) of 1.6–2.2, implying efficient aging of BC particles in polluted urban area. Our results imply a large proportion of BC-containing particles in the atmosphere, which could help towards understanding the role of BC on regional haze formation and climate forcing.

© 2020 Elsevier Ltd. All rights reserved.

1. Introduction

Although black carbon (BC) aerosols generally account for a small proportion (~5–10%) of the total mass of particulate matter with diameters smaller than 2.5 μm (PM_{2.5}) in the atmosphere, freshly emitted BC undergoes atmospheric aging that will form BC-containing particles, increasing the total mass of PM_{2.5} due to mixing with other substances (Bond and Bergstrom, 2006; Cheng et al., 2006; Peng et al., 2016; Zhang et al., 2018a,b). The effects of these BC-containing particles on regional air quality, climate, and

human health are largely different from those caused by pure BC alone (Frey et al., 2008).

Since it is difficult to obtain accurate information about what fraction and how fast BC and other types of particles are aggregated in the atmosphere (Pósfai et al., 1999), the combined climate effects of BC and coating substances are more difficult to estimate (Chýlek et al., 1995). Currently, the results of BC forcing remain debatable and are one of the key uncertainties in climate evaluation (Bond et al., 2013; Myhre et al., 2013; Stocker et al., 2013). The light absorption enhancement (E_{abs}) have been applied to quantify the radiative forcing of BC by assuming a core-shell structure of the BC-containing particles (Bond et al., 2013; Cappa et al., 2012; Cheng et al., 2006; Chung et al., 2012; Jacobson, 2001; Knox et al., 2009; Matsui et al., 2013; Moteki et al., 2007; Schwarz et al., 2006). The

[☆] This paper has been recommended for acceptance by Baoshan Xing.

* Corresponding author.

E-mail address: fang.zhang@bnu.edu.cn (F. Zhang).

E_{abs} , however, highly depends on the BC aging rate and changes in morphology and coating thickness of BC, ranging from about 1.0 to 4.0, according to different studies (Cappa et al., 2012; Chen et al., 2017; Cui et al., 2016; Lack and Cappa, 2010; Liu et al., 2017; Nakayama et al., 2014; Peng et al., 2016; Xu et al., 2016; Cheng et al., 2017).

Accurately quantifying BC-containing particles, including internally and externally mixed BC, is difficult but necessary to do to understand their aging process and presence in the atmosphere. A few studies have measured the mass, number concentration, and fraction of BC-containing particles, which are highly variable and depend on the environmental conditions (Lee et al., 2015; Massoli et al., 2015; Reddington et al., 2013; Wang et al., 2019). Different algorithms applied to data from the same area can produce inconsistent results. For example, Zhan et al. (2017b) found that the number and mass fraction of BC-containing particles accounted for only ~10–17% of the total mass based on single particle soot photometer measurements at a site near to Beijing, suggesting a minor presence in the atmosphere. However, Wang et al. (2019) reported a thick coating of BC particles observed in Beijing, which suggests that there may have been a large proportion of BC-containing particles in the atmosphere. In general, modeling of the radiative forcing of BC has the largest uncertainty in polluted urban areas (Chung et al., 2012). Accurate quantification of both the mass and number concentration/fraction of BC-containing particles in East Asia, which contains heavily polluted urban areas, is thus essential.

Most of previous studies have investigated the particles volatility properties (Cheung et al., 2016; Jiang et al., 2018; Wang et al., 2017) or inverted the number fraction of internally and externally mixed BC using the V-TDMA data (Lee et al., 2015; Massoli et al., 2015; Reddington et al., 2013; Zhan et al., 2017a). But, to our knowledge, no previous study has used such dataset to retrieve the mass concentration/fraction of internally and externally mixed BC, that reflects the contribution of BC-containing particles to $PM_{2.5}$. The SP2 measurement is generally used to determine the mass of BC-containing particles. This study retrieves and quantifies the proportion of non-BC and internally and externally mixed BC of ambient fine aerosol particles using the field-measured, size-resolved volatility shrink factor (VSF) (Cheung et al., 2016), and the mass concentration of bulk BC and the chemical composition of BC-containing particles from 28 January to February 22, 2019 at a site in the Beijing area. We focus on analyzing the importance and size dependence of internally and externally mixed BC on clean and polluted days. We also attempt to study the BC absorption enhancement using a core-shell assumption based on coating thickness on BC to reveal the role of aging degree on enhancing BC absorption.

2. Materials and methods

2.1. Site, instruments, and measurements

We conducted a field campaign from 28 January to February 22, 2019 at a site located southeast of urban Beijing (40.05°N, 116.09°E). Roads surround the sampling site with no major industrial pollution sources nearby. A series of instruments were set up and deployed in a container for simultaneously measuring the chemical and physical properties of aerosols. Size-resolved VSF (40–300 nm) and particle number size distributions (PNSD) were measured by a volatility tandem differential mobility analyzer (VTDMA) and used to determine the particle mixing state. Because this study investigates the fine mode particles below 300 nm, those refractory components, e.g. dust and sea salt, which are dominated by coarse mode particles, are negligible. At around 300–350 °C, the

refractory component in the sub micrometer size range in the continental and urban areas have been considered consisting mainly of black carbon and little charred organic material that can be negligible (Rose et al., 2006; Frey et al., 2008; Wehner et al., 2009). As a refractory component, BC remains in the particle phase upon heating, while the rest of the aerosol components tend to evaporate, resulting in a change in particle size (Cheng et al., 2009). More details about the VTDMA can be found in the supplement (Fig. S1) and in the literature (Wang et al., 2017). Auxiliary instruments included an aethalometer (AE33, Magee Scientific), and an aerosol chemical speciation monitor (ACSM). The AE33 is used to measure the mass concentration of pure BC from the change in optical attenuation at 880 nm (Zhao et al., 2017). The ACSM is used to measure the mass concentration of non-refractory aerosol components, including organics, sulfates, nitrates, ammonium, and chlorides (Li et al., 2020). Meteorological variables at different altitudes, including temperature (T), relative humidity (RH), wind speed (WS), and wind direction (WD) were also measured.

2.2. Retrieval method

In this study, we use the abbreviations Ex-BC, In-BC, and Non-BC to denote externally mixed, internally mixed, and non-BC-containing particles, respectively. The measured VSF is defined as the ratio of the diameter of the particle residual after being heated at 300 °C to the initial diameter of the sampled dry particles (Wehner et al., 2009). We classified the measured VSF values into three categories: $0.82 \leq \text{VSF} \leq 1.2$ as low volatility (LV) aerosols, considered as Ex-BC; $0.45 \leq \text{VSF} < 0.82$ as medium volatility (MV) aerosols, considered as In-BC; and $0.2 \leq \text{VSF} < 0.45$ as high volatility (HV) aerosols, considered as Non-BC (Cheng et al., 2012; Wehner et al., 2009). We then obtained the size distributions and number concentrations of In-BC, Ex-BC, and Non-BC combined with the total PNSD simultaneously measured by the VTDMA.

Fig. 1a shows the campaign average PNSDs of In-BC, Ex-BC, and Non-BC. The PNSDs of In-BC, Ex-BC and Non-BC present apparent bimodal patterns, typically with nucleation/Aitken and accumulation modes: the peak diameters are about 30 nm and 120 nm for Non-BC, 50 nm and 190 nm for In-BC, and 30 nm and 110 nm for Ex-BC. Such bimodal patterns are consistent with that previous observations in urban regions where the PNSD of fine aerosols generally is with bimodal patterns due to the multiple impacts from both local emissions/secondary conversion and regional transportation (Liu et al., 2016). We observed that the Aitken mode dominates the PNSD of Non-BC, which is likely due to that the sampling site is closer to the main traffic road and frequently impacted by urban vehicle emissions. Note that the peak diameters of the two modes for In-BC are considerably larger than that observed for Ex-BC, showing a shift to the right due to the BC aging (Jiang et al., 2018).

Based on the PNSD of Ex-BC, we then calculated the mass size distribution from the volume and density of the fresh BC (equation (1)) by assuming that the particles are spherical (Rader and McMurry, 1986). We assume that the Ex-BC effective density ranges from 0.25 to 0.45 $g\ cm^{-3}$, which are typically values for fresh BC particles according to Park et al. (2003) and Slowik et al. (2004).

$$m(\log D) = \frac{\pi}{6} \rho D^3 n(\log D) \quad (1)$$

where ρ , D , $n(\log D)$ and $m(\log D)$ are the effective density, electrical mobility diameter, and the number and mass size distributions of Ex-BC, respectively.

The retrieved campaign average mass size distribution of Ex-BC

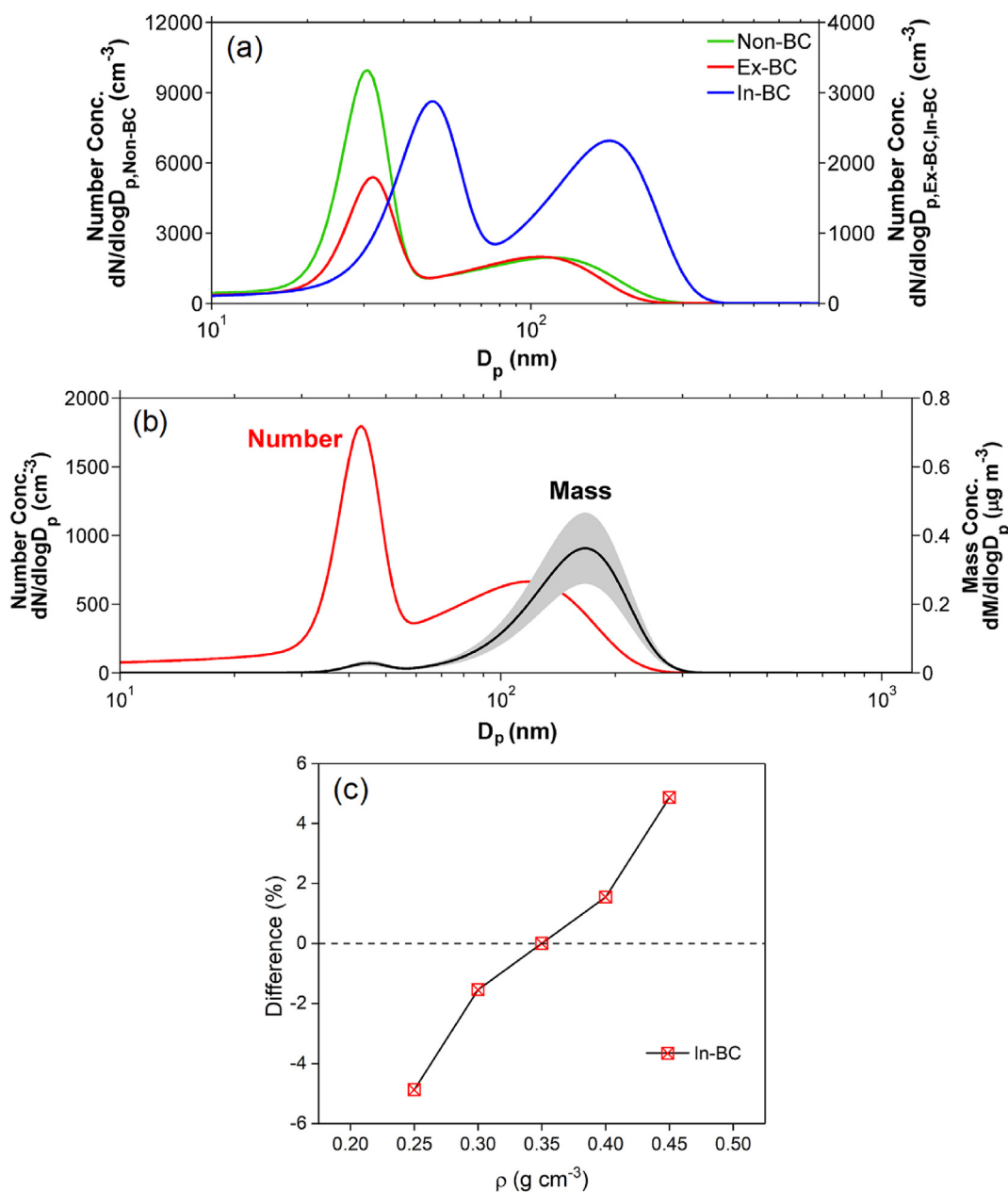


Fig. 1. (a) The campaign average number size distributions of In-BC (in blue), Ex-BC (in red), and Non-BC (in green) based on the VTDMA measurement. (b) The campaign average number and mass size distributions of Ex-BC. The grey zone represents the upper and lower limit of the calculation by applying the Ex-BC effective density of 0.25–0.45 g cm⁻³, and the black line represents the effective density of 0.35 g cm⁻³. (c) The mass fraction difference of In-BC when Ex-BC with effective density range of 0.25–0.45 g cm⁻³.

is shown in Fig. 1b. We also put the PNSD of Ex-BC in Fig. 1b for comparison. It can be seen that the Aitken mode dominates the PNSD of Ex-BC but showing negligible contribution to the particle mass. The grey zone of the mass distribution of Ex-BC represents the upper and lower limit of the calculation by applying the Ex-BC effective density of 0.45 and 0.25 g cm⁻³, respectively, and the black line is result when assuming the effective density is 0.35 g cm⁻³. The peak diameter of obtained Ex-BC mass was about 180 nm, which is close to the values observed by SP2 (~200 nm) in urban Beijing (Ding et al., 2019). Since the peak of the mass size distribution of BC typically varies between 100 and 400 nm in an urban atmosphere (Frey et al., 2008; Ding et al., 2019), the mass of BC with $D_p > 600$ nm is expected to be negligible in this study.

The total mass concentration of Ex-BC can then be calculated

from the integration of the retrieved mass size distribution:

$$M_{\text{Ex}^{\text{TT5843c571}}^{\text{ADBC}}} = \int_{D_{\text{start}}}^{D_{\text{end}}} m(\log D) d \log D \quad (2)$$

where $M_{\text{Ex}^{\text{TT5843c571}}^{\text{ADBC}}}$ is the sum of the masses for the size range of 10–600 nm.

The effective density of Ex-BC and In-BC in this study was ~0.35 g cm⁻³. The assumption of BC effective density could result in uncertainty in the retrieved mass concentrations of Ex-BC and In-BC. However, we find that the uncertainty is small, i.e., the mass concentrations of

In-BC vary within $\pm 5\%$ (Fig. 1c) by changing the effective density of Ex-BC from 0.25 to 0.45 g cm^{-3} .

The mass concentration of BC-containing particles was calculated as follows:

$$M_{\text{BC}^{\text{TT5843c571}^{\text{ADcontaining}}}} = \frac{M_{\text{pure BC}}}{\varphi_{\text{pure BC}}} \quad (3)$$

where $M_{\text{BC}^{\text{TT5843c571}^{\text{ADcontaining}}}}$ is the total mass of Ex-BC and In-BC (both BC core and coating materials), $M_{\text{pure BC}}$ is the mass concentration of pure BC obtained from the AE33 at 880 nm, and $\varphi_{\text{pure BC}}$ is the mass fraction of pure BC in the BC-containing particles. In this study, $\varphi_{\text{pure BC}}$ is assumed to be 19% on clean days and 15% on polluted days obtained by a combined measurement system which is consisted by a single-particle soot photometer (SP2) and a high-resolution aerosol mass spectrometer (HR-AMS) (Wang et al., 2019). Data measured by Wang et al. (2019) during winter of 2016 in Beijing shows that changes in $\varphi_{\text{pure BC}}$ are roughly constant during polluted and clean periods (Fig. S2). Therefore, the constant values assumed are expected to induce an insignificant uncertainty in the calculation.

Note that the mass of total BC particles will be underestimated (McMeeking et al., 2010; Schwarz et al., 2006) because of the low detection efficiency of the SP2 in measuring small BC particles. Compared to an AE33 collected in December 2016 (Wang et al., 2019), it shows that the SP2 underestimated BC mass concentration (Fig. S3) with an averaged value of 40%. Note that such result is with uncertainties because the comparison involved the factory default mass absorption cross-section (MAC) of $\sim 4.7 \text{ m}^2 \text{ g}^{-1}$ in AE33 and the calibration of SP2 deserves further investigation as well. However, in this study, the mass fraction of each component measured by the combined SP2 and HR-AMS system are thought to be reliable, so here $\varphi_{\text{pure BC}}$ is used to retrieve the total mass of internally and externally mixed BC particles.

The total mass concentration of In-BC is then calculated as $M_{\text{BC}^{\text{TT5843c571}^{\text{ADcontaining}}}}$ minus the mass concentration of Ex-BC. The mass concentration of Non-BC is calculated as the difference between the simultaneously measured mass concentrations of $\text{PM}_{2.5}$ and BC-containing particles:

$$M_{\text{In}^{\text{TT5843c571}^{\text{ADBC}}}} = M_{\text{BC}^{\text{TT5843c571}^{\text{ADcontaining}}}} - M_{\text{Ex}^{\text{TT5843c571}^{\text{ADBC}}}} \quad (4)$$

$$M_{\text{Non}^{\text{TT5843c571}^{\text{ADBC}}}} = M_{\text{PM}_{2.5}} - M_{\text{BC}^{\text{TT5843c571}^{\text{ADcontaining}}}} \quad (5)$$

where $M_{\text{In}^{\text{TT5843c571}^{\text{ADBC}}}}$ and $M_{\text{PM}_{2.5}}$ are the mass concentrations of In-BC and $\text{PM}_{2.5}$, respectively.

During the campaign, the aerosols number concentration of chemical composition (including BC) for single particles is also simultaneously measured by a single particle aerosol mass spectrometer (SPAMS) (Hexin Mass Spectrometry) (Bi et al., 2015). Although only a short time period (about one week) of synchronous data from the two instruments is obtained, this allows us to verify and evaluate the reliability of our retrieved number concentration/fraction of BC particles by the method. Because the SPAMS measures ambient particles with size range of 200–2000 nm, so the number fraction of ambient particles with 200 nm retrieved is used for comparison. As shown in Fig. 2, both the overall temporal variations and proportion for BC-containing particles measured by SPAMS and calculated from VTDMA are consistent, confirming our method are reliable for retrieve mixing state of BC in the study

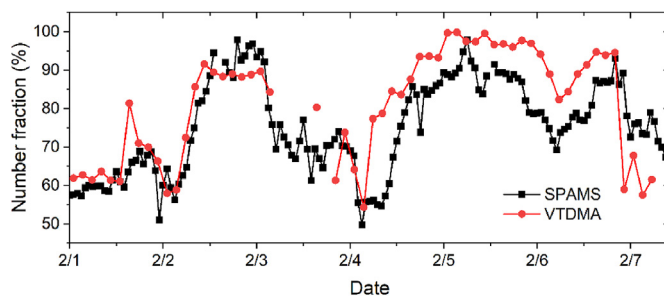


Fig. 2. Time series of number fraction of BC-containing particles measured by SPAMS (in black) and calculated from VTDMA (in red), the 200 nm particles from VTDMA are chosen.

periods. Unfortunately, more comprehensive data like size-resolved chemical composition of BC-containing particles measured by SPAMS is not available due to data sharing policy of the campaign project, and more analysis regarding to the data cannot be done in this study.

3. Results and discussion

3.1. General overview of the measurements

The field campaign time series of meteorological conditions, $\text{PM}_{2.5}$ concentration, chemical composition, and volatility (Fig. 3) show that, in general, a north wind prevailed throughout the study period. When the wind direction shifted from the north to the south, the $\text{PM}_{2.5}$ concentration increased, reaching a maximum of $348 \mu\text{g m}^{-3}$, mainly due to pollutants transported from south of the site (Gao et al., 2011; Wang et al., 2017). The average wind speed and temperature were 2.13 m s^{-1} and $0.29 \text{ }^\circ\text{C}$ during the study period, respectively. The average $\text{PM}_{2.5}$ concentration was $50.1 \mu\text{g m}^{-3}$. Observed during the field campaign were wind speeds lower than 2 m s^{-1} , conducive to the accumulation of pollutants, resulting in pollution events. The main component of $\text{PM}_{2.5}$ was organic matter, accounting for $\sim 50\%$ of the total mass of $\text{PM}_{2.5}$. When pollution events occurred, the mass fractions of nitrate and sulfate increased. The measured probability density functions of the VSF (VSF-PDF) of DMA_1 -selected particles with diameters (D_p) equal to 40, 150, and 300 nm in urban Beijing have an overall unimodal distribution. The average VSF for different D_p calculated from the VSF-PDF was ~ 0.6 , consistent with values reported by previous studies (Wang et al., 2017; Jiang et al., 2018). Here, we present the volatility of size-resolved particles under clean (characterized by $\text{PM}_{2.5}$ concentrations less than $35 \mu\text{g m}^{-3}$) and polluted (characterized by $\text{PM}_{2.5}$ concentrations greater than $150 \mu\text{g m}^{-3}$) conditions.

Fig. 4 shows size-dependent average VSF during clean and polluted periods. During the polluted period, the VSF decreased at first, then increased with increasing particle size. Small particles (40, 60, and 80 nm) had higher volatilities (i.e., low mean VSF) under clean conditions than under polluted conditions. It is possible that the particle volatility sharply increased when new particle formation (NPF) events occurred. ACSM measurements show that during NPF events, most of the newly formed particles ($>50\%$) were volatile because they were dominated by highly volatile organic particles. During polluted and clean periods, with increasing particle size, the average VSF increased, suggesting that larger particles became less volatile when they experienced aging,

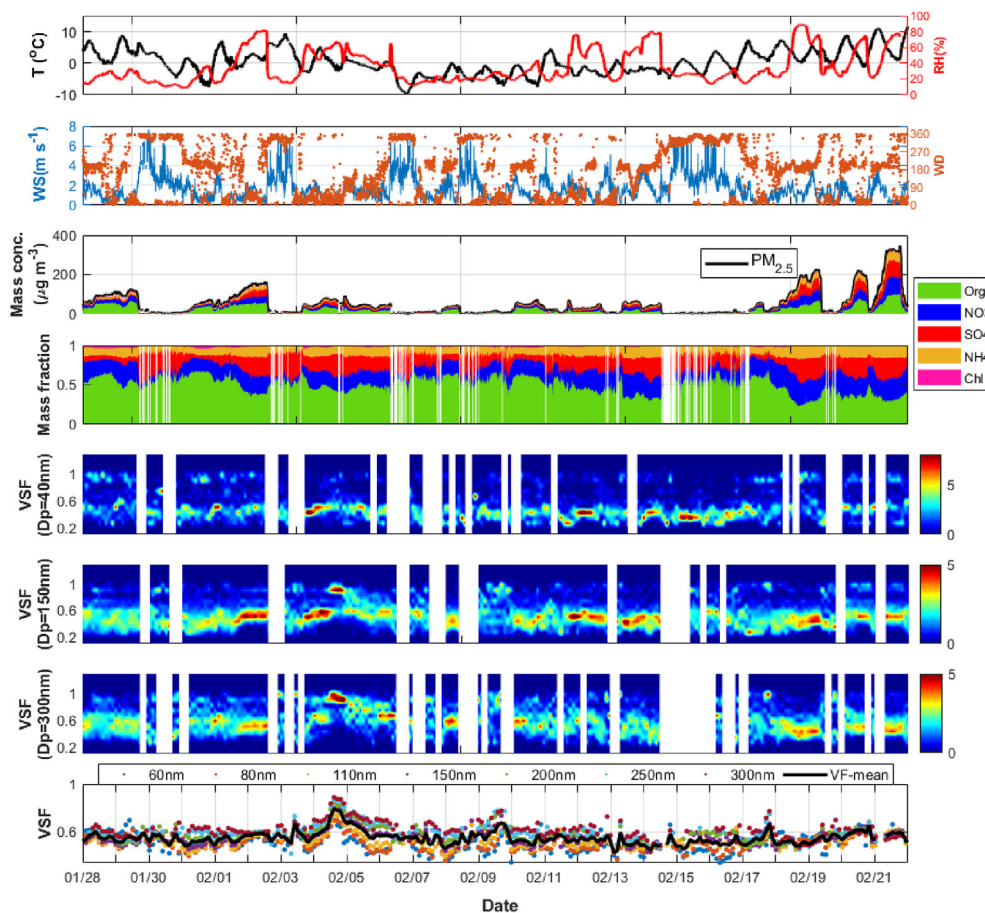


Fig. 3. Time series of (a) ambient temperature (T) and relative humidity (RH); (b) wind direction and wind speed; (c) mass concentration of $PM_{2.5}$ and its main species; (d) mass fraction of chemical composition of $PM_{2.5}$; (e–g) volatile shrink factor distributions (VSF-PDF) for 40, 150, and 300 nm particles at $T = 300$ °C; (h) mean VSF of mono-disperse aerosols with different particle size.

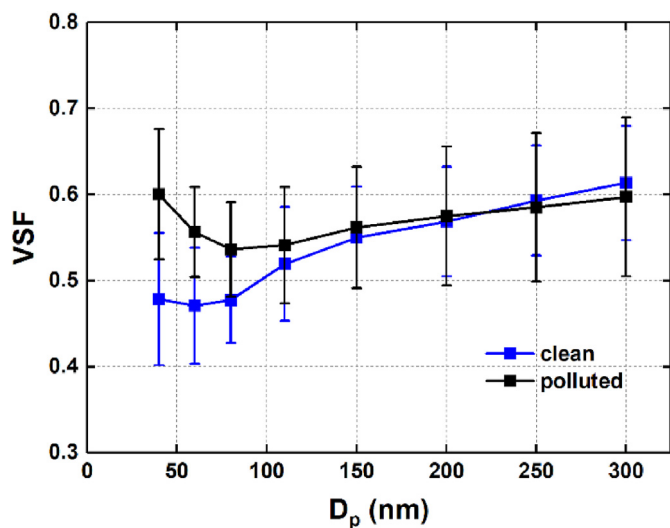


Fig. 4. Size-dependent volatility shrink factor (VSF) of fine aerosol particles under clean (in blue) and polluted (in black) conditions during the field campaign. Vertical bars show the standard deviations.

coagulation, condensation, and growth in the atmosphere (Ivleva et al., 2007; Wehner et al., 2009).

3.2. Retrieved time series of the size-resolved mixing state of atmospheric fine particles

Using VSF observations and the method described in section 2.2, we obtained the time series of number/mass concentration of Non-BC, In-BC, and Ex-BC (Fig. 5). We only present the number variations of 40- and 150-nm particles here (see Figs. S4 and S5 for the time series of other sizes). The large temporal variations in the number/mass concentration of Non-BC, In-BC, and Ex-BC were observed during the field campaign, which reflects the large fluctuations and influences from both local primary urban emissions and secondary conversions on ambient fine particles. For particles of both sizes, Ex-BC had the smallest number and mass concentrations (Fig. 5a and d), which suggests that as the atmospheric aerosols aged, most of the BC particles became mixed with other chemical compounds to form BC-containing particles. For example, for 150-nm particles, In-BC had the largest number fraction on most days during the field campaign.

Fig. 5c illustrates the distinct size dependence of the total number fractions of the BC-containing particles from clean to polluted conditions. During the clean period, small particles (<100 nm) were mostly Non-BC with number fractions ranging from 50 to 60%, and large particles (>150 nm) were mostly In-BC with number fractions greater than 60%. As the particle size increased, the number fraction of Non-BC decreased, meaning that the proportion of completely volatile and highly volatile particles decreased, which is consistent with that observed in Guangzhou

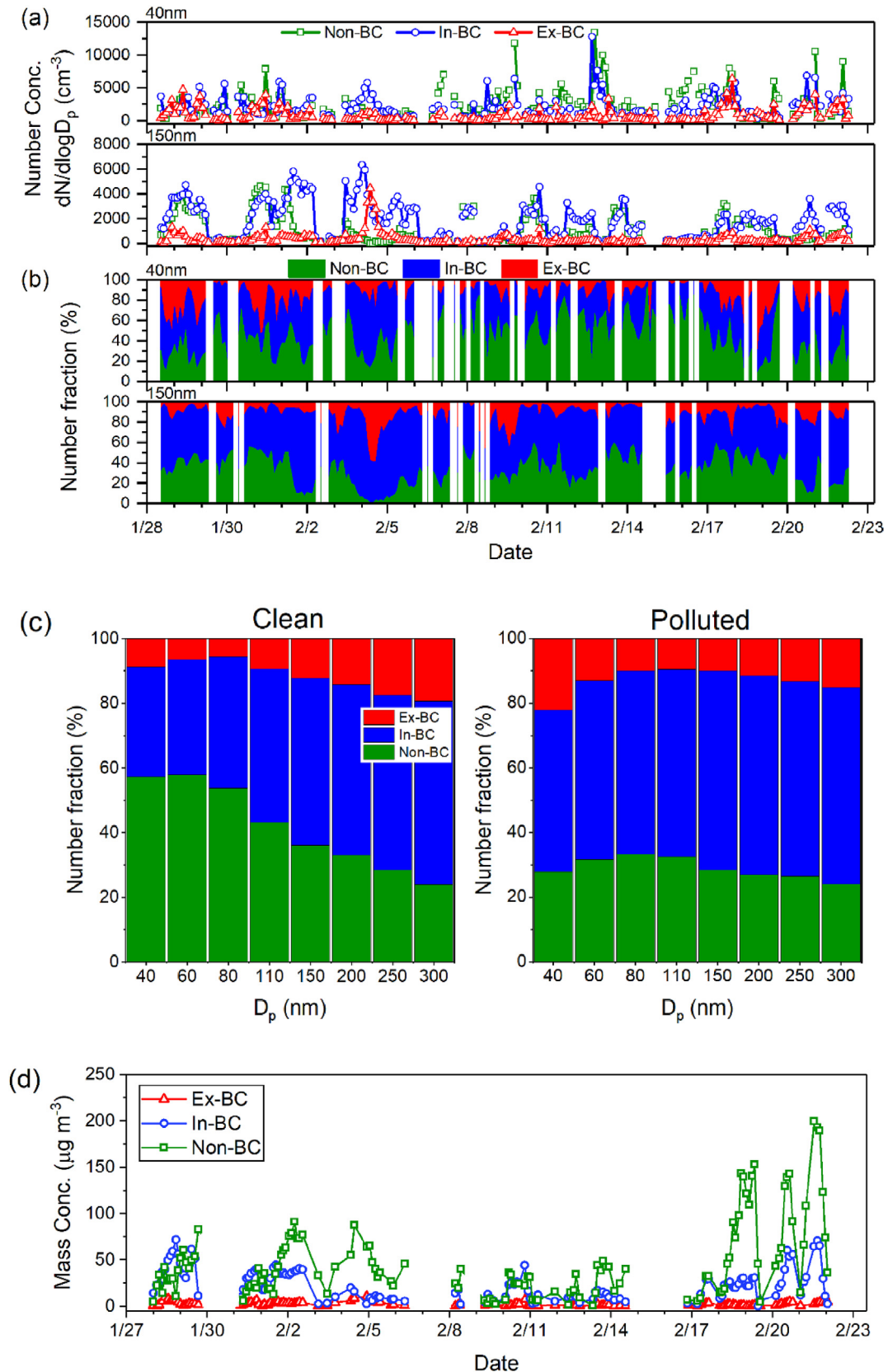


Fig. 5. Time series of (a) number concentrations and (b) number fractions of Non-BC (in green), In-BC (in blue), and Ex-BC (in red) 40- and 150-nm particles. (c) Size-resolved, campaign-averaged number fractions of Non-BC, In-BC, and Ex-BC during clean and polluted periods. (d) Time series of retrieved mass concentrations of Non-BC, In-BC and Ex-BC in $\text{PM}_{2.5}$.

(Cheung et al., 2016). Particles during the polluted period were mainly In-BC (50–62%), showing size independence. Small particles may arise mainly from the nucleation process during clean periods when primary emissions (e.g., BC and other primary organics) are small, which would thus lead to a large proportion of Non-BC in the nucleation mode on clean days. The following section discusses this further.

3.3. Number and mass fractions of BC-containing and Non-BC aerosols in the atmosphere over the site

BC-containing particles and non-BC particles. During clean periods, most ambient aerosol particles were BC-containing particles with D_p greater than 100 nm and with a total In-BC and Ex-BC number fraction of 60–78% (except for 40 nm), corresponding to a mass fraction of ~52%. This suggests that BC particles were the dominant component of ambient fine particles in the atmosphere over the site. During polluted periods, however, BC-containing particles contributed ~32% toward the mass fraction, with In-BC and Ex-BC contributing ~30% and ~2%, respectively. Compared to clean periods, the mass fraction of Non-BC during polluted periods showed a slight increase, suggesting the formation of Non-BC likely through aqueous chemistry on polluted days. Although there was a

Fig. 6 shows the number and mass concentrations/fractions of

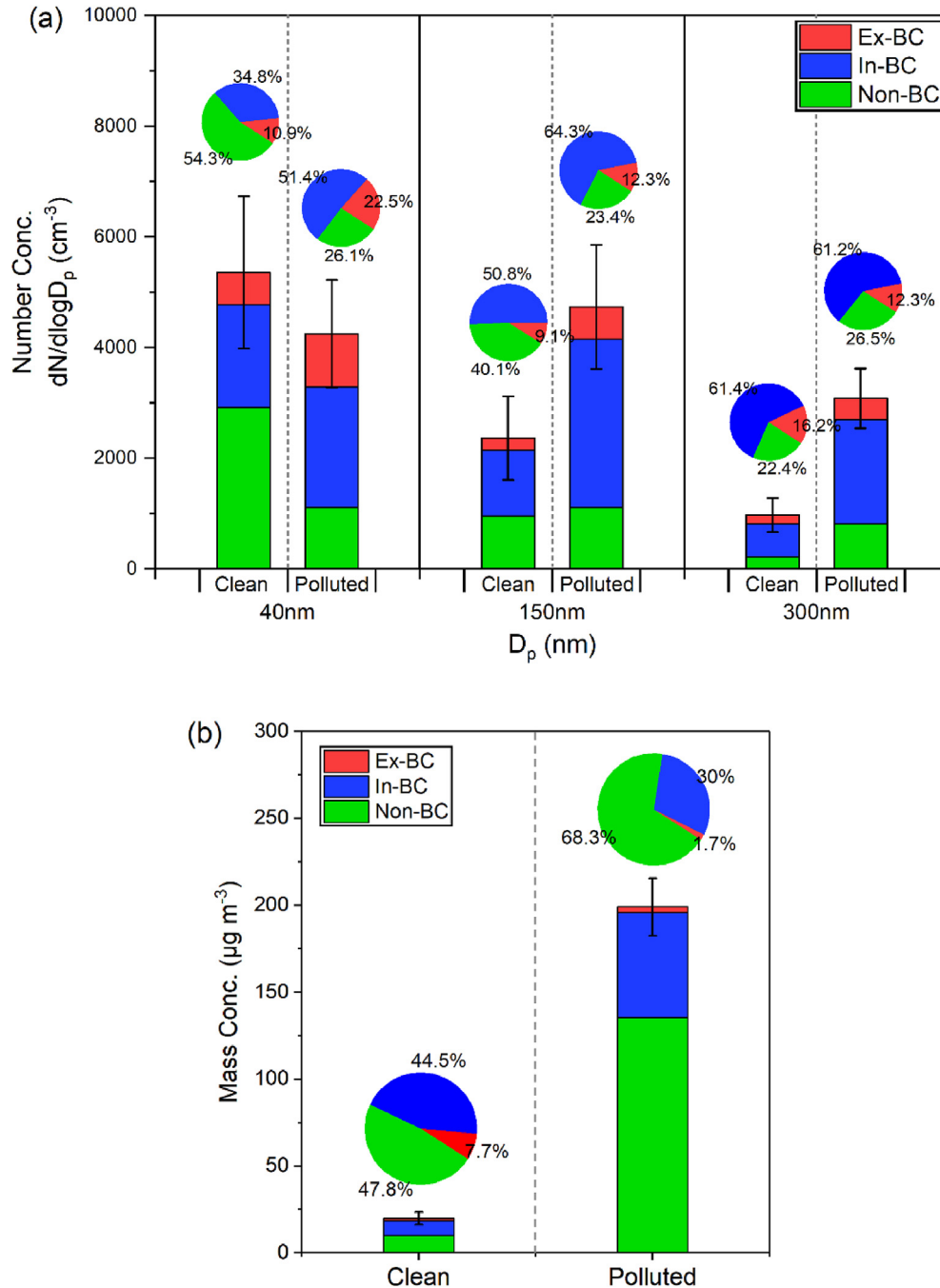


Fig. 6. Retrieved (a) number and (b) mass concentrations of Non-BC (in green), In-BC (in blue), and Ex-BC (in red) for 40-, 150-, and 300-nm particles on clean and polluted days. The number and mass fractions of Non-BC, In-BC, and Ex-BC are also included in the figure.

reduction in the mass fraction of BC-containing particles during polluted periods, the total mass fraction of BC-containing particles still accounted for one third of the fine-particle mass. For 40-nm particles, BC-containing particles accounted for a smaller number fraction (~46%) during clean periods compared to larger particles. The smaller proportion is due to the large contribution of smaller Non-BC from nucleation processes that frequently occurred on clean days. On polluted days, sources of small particles are mainly local primary traffic and cooking emissions in urban Beijing (Yu et al., 2015; Ren et al., 2018; Fan et al., 2020), which emit much fresh BC particles. This led to a larger number fraction of Ex-BC in 40-nm particles (~23%). It is worth noting that small BC particles (like from traffic) with larger surface-to-volume ratios tend to have thick coatings after aging. According to our method of dividing different mixing states of BC, these particles may be considered as Non-BC. Although such case does exist, our result basically represents the real mixing state of BC in the atmosphere by comparing with the SPAMS data (Fig. 2).

Overall, the number and mass fractions of BC-containing particles accounted for 60–78% and 32–52%, respectively, of ambient fine particles during the study period. Our results indicate that although the pure BC mass was small, typically accounting for 5–15% of total fine particles in the atmosphere (Viidanoja et al., 2002; Laborde et al., 2013; Massoli et al., 2015; Srivastava et al., 2012), the mass fraction of BC-containing aerosols in the atmosphere can be very high because of rapid aging, coagulation, and other heterogeneous processes of fresh BC particles in polluted urban areas. These atmospheric physical and chemical processes lead to the formation of thick coating materials on fresh BC (Xu et al., 2016), increasing their total mass significantly. This would not only contribute to the mass concentration of PM_{2.5} and deteriorate air quality, but it would also change the absorption and radiative forcing of BC particles and impact climate (Zhang et al., 2020). Therefore, our results suggest that BC-containing particles play a critical role in both regional haze formation and climate forcing.

As summarized in Table 1, a large number fraction of BC-containing particles, comparable with our results, was also observed in Hong Kong (Clarke et al., 2004). The mass fraction obtained in our study is consistent with that derived by Lee et al. (2015), who reported that the mass fraction of internally mixed BC particles reached ~50% in Toronto, indicating a large fraction of BC-containing aerosols. However, other studies, summarized in Table 1, reported lower number fractions or mass fractions of BC-containing particles. For example, Zhan et al. (2017a) found that the number and mass fractions of BC-containing particles were only 10–15% and 10–17%, respectively, in Xianghe, Hebei, a site very close to Beijing. Massoli et al. (2015) reported that the number and mass fractions of BC-containing particles were, on average, ~20% and 35%, respectively, in California based on SP2 and VTDMA measurements. Reddington et al. (2013), using aircraft

observations, obtained number and mass fractions of ~10% and ~14%, respectively. Overall, both the mass and number fractions vary considerably among different environments, implying large variations in BC MAC due to distinct emission sources and aging processes/rates in different regions (Xu et al., 2016). Accurately evaluating BC radiative forcing in models is thus challenging.

3.4. Coating thickness characterized by D_p/D_c ratio and calculated absorption enhancement

Previous theoretical studies have reported that coating materials on BC surfaces can significantly enhance the light absorption of BC via the lensing effect (Fuller et al., 1999; Jacobson, 2001; Lack and Cappa, 2010; Moffet and Prather, 2009). In other words, the aging degree of BC-containing particles determines their theoretical light absorption capability. However, how the aging and light absorption capability of BC particles will change under different pollution levels remains unclear. Here, the ratio D_p/D_c was used as a quantitative index to characterize the coating thickness (aging degree) of BC-containing particles. In Fig. 7a, D_p refers to the peak value of the DMA₁ selected size distribution (particles with diameters of 110 nm and 150 nm are presented as examples), and D_c refers to the peak diameter of residual particles after heating at 300 °C. Also shown are the number size distributions of ambient aerosols.

The observed BC aerosols are dominated by particles with D_p/D_c ratio of >1.6 for 110 and 150 nm particles (Fig. 7b). On average, the D_p/D_c ratio of BC particles were ~2.2 and ~1.6 at 40–110 nm and 150–300 nm respectively (Fig. S6 for the frequency distributions of other sizes), showing thinner coating material as the particle size increased. The observed large ratios of D_p/D_c suggest that the BC particles during the campaign are thickly coated with compacted structure during atmospheric aging. Therefore, to study the impact of BC aging on its absorption enhancement, we further calculate the E_{abs} at $\lambda = 550$ nm using a core-shell Mie model (Bohren and Huffman, 1983) by assuming the BC particles are spherical with fully compacted form.

The calculated E_{abs} of BC-containing particles is highly dependent on changes of D_p/D_c ratio. The maximum E_{abs} of ~2.2 is derived corresponding to D_p/D_c of ~2.1, basically consistent with that derived at sites with similar observed D_p/D_c (2.0–2.5; Fig. 8), i.e., Shouxian, Xianghe, and Toronto (Knox et al., 2009; Xu et al., 2018; Zhang et al., 2016). However, our derived E_{abs} is larger than that obtained at Guangzhou, California, and Boulder, where smaller D_p/D_c values of less than 1.5 were observed. Note that Cheng et al. (2017) observed an E_{abs} equal to ~4.2 corresponding to a D_p/D_c value of ~2.3, highlighting the uncertainties in deriving E_{abs} if the coating thickness is used. It is worth noted that, the core-shell Mie model, which assumes particles are spherical and homogeneous with core-shell structure without considering the impact of chemical composition of BC coating layer and real morphology of

Table 1
Summary of the mass and number fractions of BC-containing particles from different studies.

Site	Season	Technique	Mass fraction	Number fraction	Reference
Beijing	Winter	VTDMA	49–57%	61–80%	This study
Xianghe	Summer	SP2, VTDMA	10–17%	10–15%	Zhan et al. (2017a)
California	Early summer	SP2, VTDMA	35%	~20%	Massoli et al. (2015)
Munich	Spring	SP2	~10%	~14%	Reddington et al. (2013)
Toronto	Autumn	SP-AMS	~50%	7–11%	Lee et al. (2015)
Hong Kong	Spring	VTDMA	n/a	~85%	Clarke et al. (2004)
Leipzig	Winter	VTDMA, DMPS	~20%	~17%	Frey et al. (2008)
Paris	Winter	SP2	15–40%	~10%	Laborde et al. (2013)

n/a: not available; DMPS: differential mobility particle sizer.

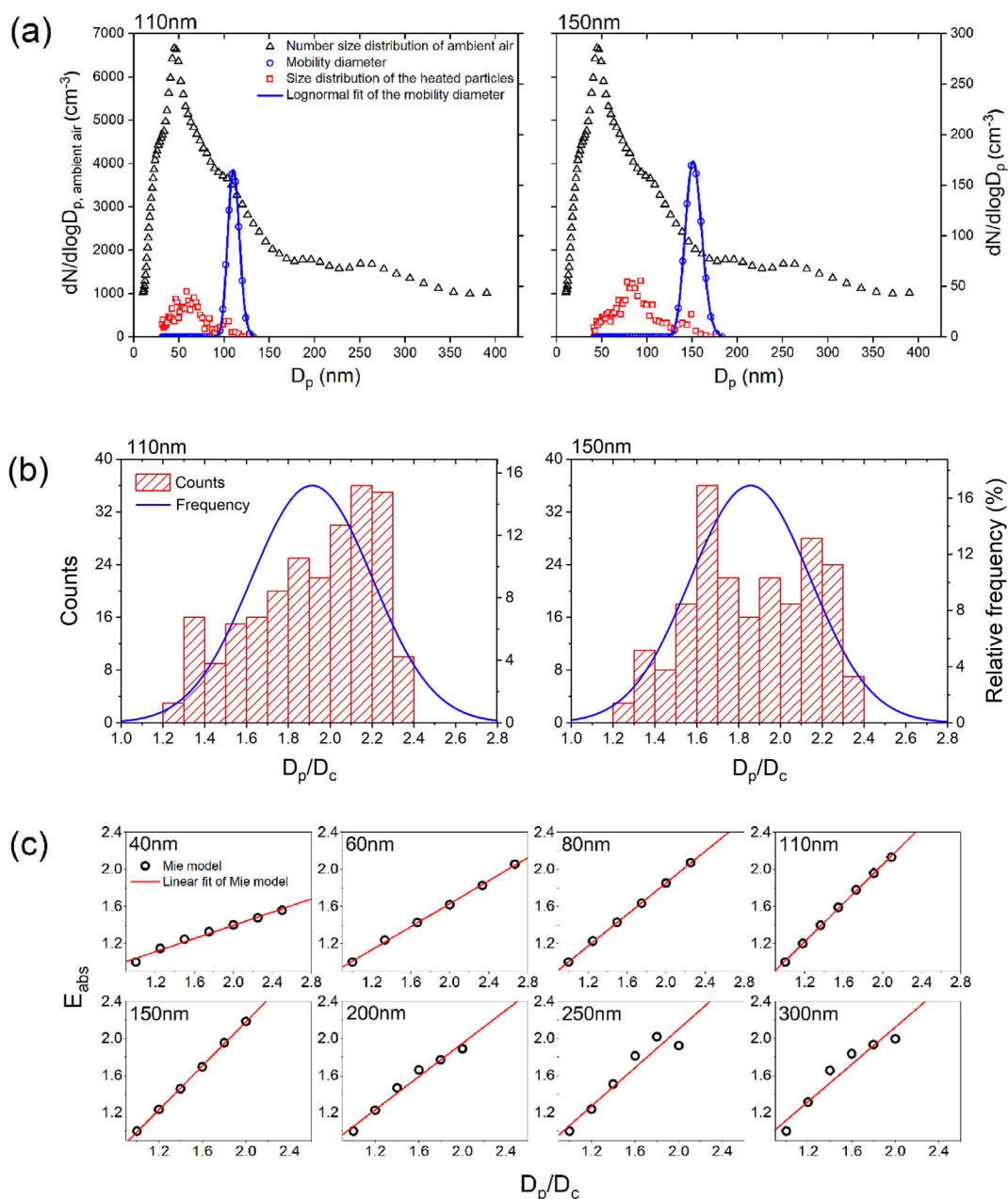


Fig. 7. (a) Number size distributions of ambient aerosols (in black), DMA₁-selected particles with D_p equal to 110 nm and 150 nm (in blue), residual particles after heating at 300 °C (in red), and the fitting curves. (b) The counts (in red) and frequency (in blue) distribution of the ratio of D_p/D_c with D_p of 110 nm and 150 nm. (c) The calculated dependence of the light absorption enhancement (E_{abs}) on the ratios of D_p/D_c .

BC in the atmosphere, is expected with some limitations.

4. Conclusions

Quantifying the proportion and absorption enhancement of black carbon (BC)-containing aerosols in the atmosphere is critical to assess their effect on air quality and climate. In this study, combining our field measured size-resolved volatility shrink factor (VSF), and mass concentrations of bulk BC and the reported the BC mass fraction in BC-containing particles in urban Beijing, we quantified the proportions of non-BC, internally, and externally mixed BC of fine aerosol particles in the atmosphere. The number fractions of BC-containing particles accounted for 60–78% of the total number concentration of ambient fine particles, with In-BC

and Ex-BC of 51–64% and 9–23%, respectively. Non-BC particles represent a large proportion (54%) of nucleated particles on clean days when new particle formation is a major source of aerosol particles. The large number fractions of BC-containing particles correspond to mass fractions of 32–52%, illustrating the critical role of BC in increasing mass concentration of PM_{2.5} through aging/heterogeneous chemical processes. In comparison of the results with previous investigations in diverse environment, we found that proportion of BC-containing particles obtained by this study are considerably or slight larger than that previous results in urban atmosphere. The uncertainty in simulating the amounts of BC-containing particles would also induce uncertainty in evaluation of the effects of BC on both regional air pollution and climate forcing. Therefore, our results are with great significance and could

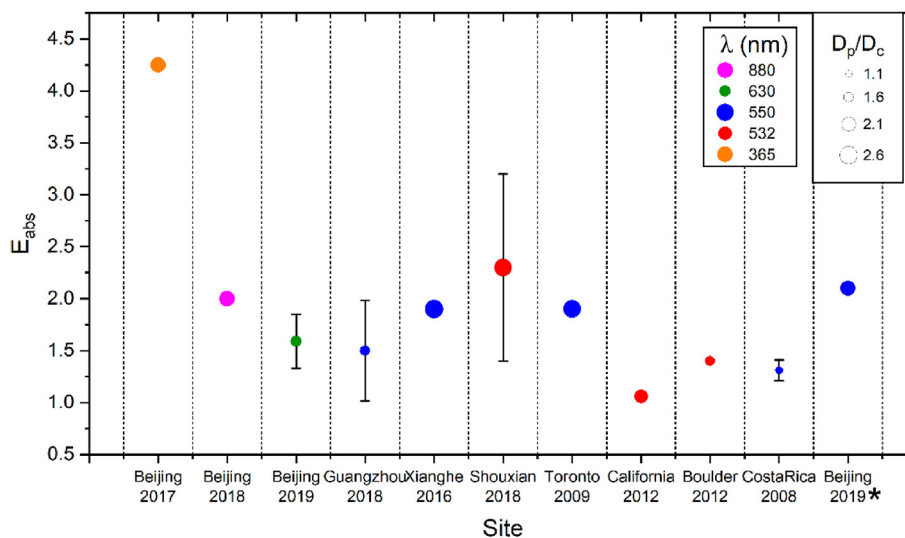


Fig. 8. E_{abs} derived at different locations around the world from previous references (Cappa et al., 2012; Knox et al., 2009; Lack et al., 2012; Schwarz et al., 2008; Wu et al., 2018; Xie et al., 2019; Xu et al., 2018; Cheng et al., 2017; Zhang et al., 2018a,b; Zhang et al., 2016). Values for the ratio D_p/D_c and wavelength are given by the size of the circles and color, respectively. The asterisk (*) represents this study. Table S1 summarizes these values given above.

help towards understanding the role of BC on regional haze formation and climate forcing.

Finally, we show that the aging degree (characterized by D_p/D_c) of BC particles can reach ~2.2 in the campaign period, implying the BC particles were thickly coated. The coating layer on BC would significantly change its hygroscopicity and CCN activity (Zhan et al., 2017b; Fan et al., 2020). The core-shell Mie model was also used to investigate the relationship of BC absorption enhancement and D_p/D_c ratio. However, the Mie model, which assumes particles are spherical and homogeneous with core-shell structure without considering the impact of chemical composition of BC coating layer and real morphology of BC in the atmosphere, is with some limitations. In the future, more comprehensive studies, including field measurements and laboratory experiments, warrant to link the refractory matter to specific sources, and the field-measured absorption enhancement to chemical compositions of the coating materials and BC morphology. This is critical to evaluate the effects on BC mixing state and its optical properties quantitatively to reduce the uncertainty in evaluation of the effects of BC on both regional air pollution and climate forcing.

Declaration of competing interest

The authors declare that they have no known competing financial interests or personal relationships that could have appeared to influence the work reported in this paper.

CRediT authorship contribution statement

Lu Chen: Formal analysis, Writing - original draft. **Fang Zhang:** Conceptualization, Formal analysis, Writing - original draft. **Xinming Wang:** Writing - review & editing. **Yele Sun:** Writing - review & editing. **Zhanqing Li:** Writing - review & editing.

Acknowledgments

This work was funded by NSFC research projects (41975174, 41675141 and 91544217), and the National Basic Research Program of China (2017YFC1501702). We thank all participants in the field campaigns for their tireless work and cooperation. The data used

for this paper are available on request to the corresponding author. The authors declare no competing financial interest.

Appendix A. Supplementary data

Supplementary data to this article can be found online at <https://doi.org/10.1016/j.envpol.2020.114507>.

References

- Bi, X., Dai, S., Zhang, G., Qiu, N., Li, M., Wang, X., Chen, D., Peng, P., Sheng, G., Fu, J., Zhou, Z., 2015. Real-time and single-particle volatility of elemental carbon-containing particles in the urban area of Pearl River Delta region, China. *Atmos. Environ.* 118, 194–202.
- Bohren, C.F., Huffman, D.R., 1983. *Absorption and Scattering of Light by Small Particles*. Wiley Interscience, New York.
- Bond, T.C., Bergstrom, R.W., 2006. Light absorption by carbonaceous particles: an investigative review. *Aerosol Sci. Technol.* 40, 27–67.
- Bond, T.C., Doherty, S.J., Fahey, D.W., Forster, P.M., Berntsen, T., DeAngelo, B.J., Flanner, M.G., Ghan, S., Kärcher, B., Koch, D., Kinne, S., Kondo, Y., Quinn, P.K., Sarofim, M.C., Schultz, M.G., Schulz, M., Venkataraman, C., Zhang, H., Zhang, S., Bellouin, N., Guttikunda, S.K., Hopke, P.K., Jacobson, M.Z., Kaiser, J.W., Klimont, Z., Lohmann, U., Schwarz, J.P., Shindell, D., Storelvmo, T., Warren, S.G., Zender, C.S., 2013. Bounding the role of black carbon in the climate system: a scientific assessment. *J. Geophys. Res.: Atmosphere* 118, 5380–5552.
- Cappa, C.D., Onasch, T.B., Massoli, P., Worsnop, D.R., Bates, T.S., Cross, E.S., Davidovits, P., Hakala, J., Hayden, K.L., Jobson, B.T., Kolesar, K.R., Lack, D.A., Lerner, B.M., Li, S.-M., Mellon, D., Nuaaman, I., Olfert, J.S., Petäjä, T., Quinn, P.K., Song, C., Subramanian, R., Williams, E.J., Zaveri, R.A., 2012. Radiative absorption enhancements due to the mixing state of atmospheric black carbon. *Science* 337, 1078–1081.
- Chýlek, P., Videen, G., Ngo, D., Pinnick, R.G., Klett, J.D., 1995. Effect of black carbon on the optical properties and climate forcing of sulfate aerosols. *J. Geophys. Res.: Atmosphere* 100, 16325–16332.
- Chen, B., Bai, Z., Cui, X., Chen, J., Andersson, A., Gustafsson, Ö., 2017. Light absorption enhancement of black carbon from urban haze in Northern China winter. *Environ. Pollut.* 221, 418–426.
- Cheng, Y.F., Berghof, M., Garland, R.M., Wiedensohler, A., Wehner, B., Müller, T., Su, H., Zhang, Y.H., Achtert, P., Nowak, A., Pöschl, U., Zhu, T., Hu, M., Zeng, L.M., 2009. Influence of soot mixing state on aerosol light absorption and single scattering albedo during air mass aging at a polluted regional site in north-eastern China. *J. Geophys. Res.: Atmosphere* 114, 153–155.
- Cheng, Y.F., Eichler, H., Wiedensohler, A., Heintzenberg, J., Zhang, Y.H., Hu, M., Herrmann, H., Zeng, L.M., Liu, S., Gnauk, T., Brüggemann, E., He, L.Y., 2006. Mixing state of elemental carbon and non-light-absorbing aerosol components derived from in situ particle optical properties at Xinken in Pearl River Delta of China. *J. Geophys. Res.: Atmosphere* 111, D20204.
- Cheng, Y.F., Su, H., Rose, D., Gunthe, S.S., Berghof, M., Wehner, B., Achtert, P., Nowak, A., Takegawa, N., Kondo, Y., Shiraiwa, M., Gong, Y.G., Shao, M., Hu, M., Zhu, T., Zhang, Y.H., Carmichael, G.R., Wiedensohler, A., Andreae, M.O.,

- Pöschl, U., 2012. Size-resolved measurement of the mixing state of soot in the megacity Beijing, China: diurnal cycle, aging and parameterization. *Atmos. Chem. Phys.* 12, 4477–4491.
- Cheng, Y., He, K.B., Engling, G., Weber, R., Liu, J.M., Du, Z.Y., Dong, S.P., 2017. Brown and black carbon in Beijing aerosol: implications for the effects of brown coating on light absorption by black carbon. *Sci. Total Environ.* 599–600, 1047–1055.
- Cheung, H.H.Y., Tan, H., Xu, H., Li, F., Wu, C., Yu, J.Z., Chan, C.K., 2016. Measurements of non-volatile aerosols with a VTDMA and their correlations with carbonaceous aerosols in Guangzhou, China. *Atmos. Chem. Phys.* 16, 8431–8446.
- Chung, C.E., Ramanathan, V., Decremer, D., 2012. Observationally constrained estimates of carbonaceous aerosol radiative forcing. *Proc. Natl. Acad. Sci.* 109, 11624–11629.
- Clarke, A.D., Shinzuka, Y., Kapustin, V.N., Howell, S., Huebert, B., Doherty, S., Anderson, T., Covert, D., Anderson, J., Hua, X., Moore II, K.G., McNaughton, C., Carmichael, G., Weber, R., 2004. Size distributions and mixtures of dust and black carbon aerosol in Asian outflow: physicochemistry and optical properties. *J. Geophys. Res.: Atmosphere* 109, D15S09.
- Cui, X., Wang, X., Yang, L., Chen, B., Chen, J., Andersson, A., Gustafsson, Ö., 2016. Radiative absorption enhancement from coatings on black carbon aerosols. *Sci. Total Environ.* 551–552, 51–56.
- Ding, S., Liu, D., Zhao, D., Hu, K., Tian, P., Zhou, W., Huang, M., Yang, Y., Wang, F., Sheng, J., Liu, Q., Kong, S., Cui, P., Huang, Y., He, H., Coe, H., Ding, D., 2019. Size-related physical properties of black carbon in the lower atmosphere over Beijing and Europe. *Environ. Sci. Technol.* 53, 11112–11121.
- Fan, X., Liu, J., Zhang, F., Chen, L., Conlins, D., Xu, W., Jin, X., Ren, J., Wang, Y., Wu, H., Li, S., Sun, Y., Li, Z., 2020. Contrasting size-resolved hygroscopicity of fine particles derived by HTDMA and HR-ToF-AMS measurements between summer and winter in Beijing: the impacts of aerosol aging and local emissions. *Atmos. Chem. Phys.* 20, 915–929. <https://doi.org/10.5194/acp-20-915-2020>.
- Frey, A., Rose, D., Wehner, B., Müller, T., Cheng, Y., Wiedensohler, A., Virkkula, A., 2008. Application of the volatility-TDMA technique to determine the number size distribution and mass concentration of less volatile particles. *Aerosol Sci. Technol.* 42, 817–828.
- Fuller, K.A., Malm, W.C., Kreidenweis, S.M., 1999. Effects of mixing on extinction by carbonaceous particles. *J. Geophys. Res.: Atmosphere* 104, 15941–15954.
- Gao, Y., Liu, X., Zhao, C., Zhang, M., 2011. Emission controls versus meteorological conditions in determining aerosol concentrations in Beijing during the 2008 Olympic Games. *Atmos. Chem. Phys.* 11, 12437–12451.
- Ivleva, N.P., Messerer, A., Yang, X., Niessner, R., Pöschl, U., 2007. Raman micro-spectroscopic analysis of changes in the chemical structure and reactivity of soot in a diesel Exhaust aftertreatment model system. *Environ. Sci. Technol.* 41, 3702–3707.
- Jacobson, M.Z., 2001. Strong radiative heating due to the mixing state of black carbon in atmospheric aerosols. *Nature* 409, 695–697.
- Jiang, S., Ye, X., Wang, R., Tao, Y., Ma, Z., Yang, X., Chen, J., 2018. Measurements of nonvolatile size distribution and its link to traffic soot in urban Shanghai. *Sci. Total Environ.* 615, 452–461.
- Knox, A., Evans, G.J., Brook, J.R., Yao, X., Jeong, C.H., Godri, K.J., Sabaliauskas, K., Slowik, J.G., 2009. Mass absorption cross-section of ambient black carbon aerosol in relation to chemical age. *Aerosol Sci. Technol.* 43, 522–532.
- Laborde, M., Crippa, M., Tritscher, T., Jurányi, Z., Decarlo, P.F., Temime-Roussel, B., Marchand, N., Eckhardt, S., Stohl, A., Baltensperger, U., Prévôt, A.S.H., Weingartner, E., Gysel, M., 2013. Black carbon physical properties and mixing state in the European megacity Paris. *Atmos. Chem. Phys.* 13, 5831–5856.
- Lack, D.A., Cappa, C.D., 2010. Impact of brown and clear carbon on light absorption enhancement, single scatter albedo and absorption wavelength dependence of black carbon. *Atmos. Chem. Phys.* 10, 4207–4220.
- Lee, A.K.Y., Willis, M.D., Healy, R.M., Onasch, T.B., Abbatt, J.P.D., 2015. Mixing state of carbonaceous aerosol in an urban environment: single particle characterization using the soot particle aerosol mass spectrometer (SP-AMS). *Atmos. Chem. Phys.* 15, 1823–1841.
- Li, S., Zhang, F., Jin, X., Sun, Y., Wu, H., Xie, C., Chen, L., Liu, J., Wu, T., Jiang, S., Cribb, M., Li, Z., 2020. Characterizing the ratio of nitrate to sulfate in ambient fine particles of urban Beijing during 2018–2019. *Atmos. Environ.* (submitted for publication).
- Liu, D., Whitehead, J., Alfara, M.R., Reyes-Villegas, E., Spracklen, Dominick V., Reddington, Carly L., Kong, S., Williams, Paul I., Ting, Y.-C., Haslett, S., Taylor, Jonathan W., Flynn, Michael J., Morgan, William T., McFiggans, G., Coe, H., Allan, James D., 2017. Black-carbon absorption enhancement in the atmosphere determined by particle mixing state. *Nat. Geosci.* 10, 184–188.
- Liu, Z., Wang, Y., Hu, B., Ji, D., Zhang, J., Wu, F., Wan, X., Wang, Y., 2016. Source appointment of fine particle number and volume concentration during severe haze pollution in Beijing in January 2013. *Environ. Sci. Pollut. Res. Int.* 23, 6845–6860.
- Massoli, P., Onasch, T.B., Cappa, C.D., Nuamaan, I., Hakala, J., Hayden, K., Li, S.M., Sueper, D.T., Bates, T.S., Quinn, P.K., Jayne, J.T., Worsnop, D.R., 2015. Characterization of black carbon-containing particles from soot particle aerosol mass spectrometer measurements on the R/V Atlantis during CalNex 2010. *J. Geophys. Res.: Atmosphere* 120, 2575–2593.
- Matsui, H., Koike, M., Kondo, Y., Moteki, N., Fast, J.D., Zaveri, R.A., 2013. Development and validation of a black carbon mixing state resolved three-dimensional model: aging processes and radiative impact. *J. Geophys. Res.: Atmosphere* 118, 2304–2326.
- McMeeking, G.R., Hamburger, T., Liu, D., Flynn, M., Morgan, W.T., Northway, M., Highwood, E.J., Krejci, R., Allan, J.D., Minikin, A., Coe, H., 2010. Black carbon measurements in the boundary layer over western and northern Europe. *Atmos. Chem. Phys.* 10, 9393–9414.
- Moffet, R.C., Prather, K.A., 2009. In-situ measurements of the mixing state and optical properties of soot with implications for radiative forcing estimates. *Proc. Natl. Acad. Sci.* 106, 11872–11877.
- Moteki, N., Kondo, Y., Miyazaki, Y., Takegawa, N., Komazaki, Y., Kurata, G., Shirai, T., Blake, D.R., Miyakawa, T., Koike, M., 2007. Evolution of mixing state of black carbon particles: aircraft measurements over the western Pacific in March 2004. *Geophys. Res. Lett.* 34, L11803.
- Nakayama, T., Ikeda, Y., Sawada, Y., Setoguchi, Y., Ogawa, S., Kawana, K., Mochida, M., Ikemori, F., Matsumoto, K., Matsumi, Y., 2014. Properties of light-absorbing aerosols in the Nagoya urban area, Japan, in August 2011 and January 2012: contributions of brown carbon and lensing effect. *J. Geophys. Res.: Atmosphere* 119, 12,721–712,739.
- Pósfai, M., Anderson, J., Buseck, P., Sievering, H., 1999. Soot and sulfate particles in the remote marine troposphere. *J. Geophys. Res.* 104, 21685–21693.
- Park, K., Cao, F., Kittelson, D.B., McMurry, P.H., 2003. Relationship between particle mass and mobility for diesel Exhaust particles. *Environ. Sci. Technol.* 37, 577–583.
- Peng, J., Hu, M., Guo, S., Du, Z., Zheng, J., Shang, D., Levy Zamora, M., Zeng, L., Shao, M., Wu, Y.-S., Zheng, J., Wang, Y., Glen, C.R., Collins, D.R., Molina, M.J., Zhang, R., 2016. Markedly enhanced absorption and direct radiative forcing of black carbon under polluted urban environments. *Proc. Natl. Acad. Sci.* 113, 4266–4271.
- Rader, D.J., McMurry, P.H., 1986. Application of the tandem differential mobility analyzer to studies of droplet growth or evaporation. *J. Geophys. Res.* 17, 771–787.
- Reddington, C.L., McMeeking, G., Mann, G.W., Coe, H., Frontoso, M.G., Liu, D., Flynn, M., Spracklen, D.V., Carslaw, K.S., 2013. The mass and number size distributions of black carbon aerosol over Europe. *Atmos. Chem. Phys.* 13, 4917–4939.
- Ren, J., Zhang, F., Wang, Y., Conlins, D., Fan, X., Jin, X., Xu, W., Sun, Y., Cribb, M., Li, Z., 2018. Using different assumptions of aerosol mixing state and chemical composition to predict CCN concentrations based on field measurements in urban Beijing. *Atmos. Chem. Phys.* 18, 6907–6921. <https://doi.org/10.5194/acp-18-6907-2018>.
- Rose, D., Wehner, B., Ketzel, M., Engler, C., Voigtländer, J., Tuch, T., Wiedensohler, A., 2006. Atmospheric number size distributions of soot particles and estimation of emission factors. *Atmos. Chem. Phys.* 6, 1021–1031.
- Schwarz, J.P., Gao, R.S., Fahey, D.W., Thomson, D.S., Watts, L.A., Wilson, J.C., Reeves, J.M., Darbeheshti, M., Baumgardner, D.G., Kok, G.L., Chung, S.H., Schulz, M., Hendricks, J., Lauer, A., Kärcher, B., Slowik, J.G., Rosenlof, K.H., Thompson, T.L., Langford, A.O., Loewenstein, M., Aikin, K.C., 2006. Single-particle measurements of midlatitude black carbon and light-scattering aerosols from the boundary layer to the lower stratosphere. *J. Geophys. Res.: Atmosphere* 111, D16207.
- Slowik, J.G., Stainken, K., Davidovits, P., Williams, L.R., Jayne, J.T., Kolb, C.E., Worsnop, D.R., Rudich, Y., DeCarlo, P.F., Jimenez, J.L., 2004. Particle morphology and density characterization by combined mobility and aerodynamic diameter measurements. Part 2: application to combustion-generated soot aerosols as a function of fuel Equivalence ratio. *Aerosol Sci. Technol.* 38, 1206–1222.
- Srivastava, V., Ram, K., Pant, P., Hegde, P., Joshi, H., 2012. Black carbon aerosols over central Himalayas: implications to climate forcing. *Environ. Res. Lett.* 7, 14002.
- Stocker, T.F., Qin, D., Plattner, G.K., Tignor, M., Allen, S.K., Boschung, J., Nauels, A., Xia, Y., Bex, V., Midgley, P.M., 2013. Climate Change 2013: The Physical Science Basis. Intergovernmental Panel on Climate Change, Working Group I Contribution to the IPCC Fifth Assessment Report (AR5). Cambridge University Press, New York.
- Viidanoja, J., Sillanpää, M., Laakia, J., Kerminen, V.-M., Hillamo, R., Aarnio, P., Koskentalo, T., 2002. Organic and black carbon in PM_{2.5} and PM₁₀: 1 year of data from an urban site in Helsinki, Finland. *Atmos. Environ.* 36, 3183–3193.
- Wang, J., Liu, D., Ge, X., Wu, Y., Shen, F., Chen, M., Zhao, J., Xie, C., Wang, Q., Xu, W., Zhang, J., Hu, J., Allan, J., Joshi, R., Fu, P., Coe, H., Sun, Y., 2019. Characterization of black carbon-containing fine particles in Beijing during wintertime. *Atmos. Chem. Phys.* 19, 447–458.
- Wang, Y., Zhang, F., Li, Z., Tan, H., Xu, H., Ren, J., Zhao, J., Du, W., Sun, Y., 2017. Enhanced hydrophobicity and volatility of submicron aerosols under severe emission control conditions in Beijing. *Atmos. Chem. Phys.* 17, 5239–5251.
- Wehner, B., Berghof, M., Cheng, Y.F., Achtert, P., Birmili, W., Nowak, A., Wiedensohler, A., Garland, R.M., Pöschl, U., Hu, M., Zhu, T., 2009. Mixing state of nonvolatile aerosol particle fractions and comparison with light absorption in the polluted Beijing region. *J. Geophys. Res.: Atmosphere* 114, D00G17.
- Wu, C., Wu, D., Yu, J.Z., 2018. Quantifying black carbon light absorption enhancement with a novel statistical approach. *Atmos. Chem. Phys.* 18, 289–309.
- Xie, C., Xu, W., Wang, J., Liu, D., Ge, X., Zhang, Q., Wang, Q., Du, W., Zhao, J., Zhou, W., Li, J., Fu, P., Wang, Z., Worsnop, D., Sun, Y., 2019. Light absorption enhancement of black carbon in urban Beijing in summer. *Atmos. Environ.* 213, 499–504.
- Xu, X., Zhao, W., Zhang, Q., Wang, S., Fang, B., Chen, W., Venables, D.S., Wang, X., Pu, W., Wang, X., Gao, X., Zhang, W., 2016. Optical properties of atmospheric fine particles near Beijing during the HOPE-J3A campaign. *Atmos. Chem. Phys.* 16, 6421–6439.
- Yu, N., Zhu, Y., Xie, X., Yan, C., Zhu, T., Zheng, M., 2015. Characterization of ultrafine particles and other traffic related pollutants near roadways in Beijing. *Aerosol Air Qual. Res.* 15, 1261–1269.

- Zhang, F., Wang, Y., Peng, J., Chen, L., Sun, Y., Duan, L., Ge, X., Li, Y., Zhao, J., Liu, C., Zhang, X., Zhang, G., Pan, Y., Wang, Y., Zhang, A.L., Ji, Y., Wang, G., Hu, M., Molina, M.J., Zhang, R., 2020. An unexpected catalyst dominates formation and radiative forcing of regional haze. *Proc. Natl. Acad. Sci.* 117 (8), 3960–3966. <https://doi.org/10.1073/pnas.1919343117>, 201919343.
- Zhang, Y., Favez, O., Canonaco, F., Liu, D., Močnik, G., Amodeo, T., Sciare, J., Prévôt, A.S.H., Gros, V., Albinet, A., 2018a. Evidence of major secondary organic aerosol contribution to lensing effect black carbon absorption enhancement. *npj Clim. Atmos. Sci.* 1, 47.
- Zhang, Y., Su, H., Kecorius, S., Wang, Z., Hu, M., Zhu, T., He, K., Wiedensohler, A., Zhang, Q., Cheng, Y., 2017b. Mixing state of refractory black carbon of the north China plain regional aerosol combining a single particle soot photometer and a volatility tandem differential mobility analyzer. *Atmos. Chem. Phys. Discuss.* 2017, 1–27.
- Zhang, Y., Zhang, Q., Cheng, Y., Su, H., Li, H., Li, M., Zhang, X., Ding, A., He, K., 2018b. Amplification of light absorption of black carbon associated with air pollution. *Atmos. Chem. Phys.* 18, 9879–9896.
- Zhang, F., Wang, Y., Peng, J., Ren, J., Collins, D., Zhang, R., Sun, Y., Yang, X., Li, Z., 2017a. Uncertainty in predicting CCN activity of aged and primary aerosols. *J. Geophys. Res. Atmos.* 122 (21), 11723–11736. <https://doi.org/10.1002/2017JD027058>.
- Zhang, Y., Zhang, Q., Cheng, Y., Su, H., Kecorius, S., Wang, Z., Wu, Z., Hu, M., Zhu, T., Wiedensohler, A., He, K., 2016. Measuring the morphology and density of internally mixed black carbon with SP2 and VTDMA: new insight into the absorption enhancement of black carbon in the atmosphere. *Atmos. Meas. Tech.* 9, 1833–1843.
- Zhao, J., Du, W., Zhang, Y., Wang, Q., Chen, C., Xu, W., Han, T., Wang, Y., Fu, P., Wang, Z., Li, Z., Sun, Y., 2017. Insights into aerosol chemistry during the 2015 China Victory Day parade: results from simultaneous measurements at ground level and 260 m in Beijing. *Atmos. Chem. Phys.* 17, 3215–3232.